The Astrophysical Journal, 822:57 (8pp), 2016 May 1 doi:10.3847/0004-637X/822/1/57

NUSTAR AND *XMM-NEWTON* OBSERVATIONS OF 1E1743.1-2843: INDICATIONS OF A NEUTRON STAR LMXB NATURE OF THE COMPACT OBJECT

Simone Lotti[1], Lorenzo Natalucci[1], Kaya Mori[2], Frederick K. Baganoff[3], Steven E. Boggs[4], Finn E. Christensen[5], William W. Craig[4,3], Charles J. Hailey[3], Fiona A. Harrison[6], Jaesub Hong[7], Roman A. Krivonos[4,8], Farid Rahoui[9,10], Daniel Stern[11], John A. Tomsick[4], Shuo Zhang[3], and William W. Zhang[12]
[1] INAF-IAPS Roma, Via fosso del cavaliere 100, Rome I-00133, Italy; simone.lotti@iaps.inaf.it
[2] Columbia Astrophysics Laboratory, Columbia University, New York, NY 10027, USA
[3] MIT Kavli Institute for Astrophysics and Space Research, Cambridge, MA 02139, USA
[4] Space Sciences Laboratory, 7 Gauss Way, University of California, Berkeley, CA 94720-7450, USA
[5] DTU Space, National Space Institute, Elektrovej 327, DK-2800 Lyngby, Denmark
[6] Cahill Center for Astronomy and Astrophysics, Caltech, Pasadena, CA 91125, USA
[7] Harvard-Smithsonian Center for Astrophysics, 60 Garden Street, Cambridge, MA 02138, USA
[8] Space Research Institute, Russian Academy of Sciences, Profsoyuznaya 84/32, 117997 Moscow, Russia
[9] Department of Astronomy, Harvard University, 60 Garden Street, Cambridge, MA 02138, USA
[10] European Southern Observatory, Karl Schwarzschild-Strasse 2, D-85748 Garching bei München, Germany
[11] Jet Propulsion Laboratory, California Institute of Technology, Pasadena, CA 91109, USA
[12] NASA Goddard Space Flight Center, Greenbelt, MD 20771, USA
Received 2015 October 16; accepted 2016 March 4; published 2016 May 5

ABSTRACT

We report on the results of *NuSTAR* and *XMM-Newton* observations of the persistent X-ray source 1E1743.1-2843, located in the Galactic Center region. The source was observed between 2012 September and October by *NuSTAR* and *XMM-Newton*, providing almost simultaneous observations in the hard and soft X-ray bands. The high X-ray luminosity points to the presence of an accreting compact object. We analyze the possibilities of this accreting compact object being either a neutron star (NS) or a black hole, and conclude that the joint *XMM-Newton* and *NuSTAR* spectrum from 0.3 to 40 keV fits a blackbody spectrum with $kT \sim 1.8$ keV emitted from a hot spot or an equatorial strip on an NS surface. This spectrum is thermally Comptonized by electrons with $kT_e \sim 4.6$ keV. Accepting this NS hypothesis, we probe the low-mass X-ray binary (LMXB) or high-mass X-ray binary (HMXB) nature of the source. While the lack of Type-I bursts can be explained in the LMXB scenario, the absence of pulsations in the 2 mHz–49 Hz frequency range, the lack of eclipses and of an IR companion, and the lack of a K_α line from neutral or moderately ionized iron strongly disfavor interpreting this source as a HMXB. We therefore conclude that 1E1743.1-2843 is most likely an NS-LMXB located beyond the Galactic Center. There is weak statistical evidence for a soft X-ray excess which may indicate thermal emission from an accretion disk. However, the disk normalization remains unconstrained due to the high hydrogen column density ($N_{\rm H} \sim 1.6 \times 10^{23}$ cm^{-2}).

Key words: accretion, accretion disks – stars: neutron – X-rays: binaries – X-rays: individual (1E1743.1-2843)

1. INTRODUCTION

The X-ray source 1E1743.1-2843 was discovered during the first soft X-ray imaging observation of the Galactic Center, which was performed by the *Einstein Observatory* (Watson et al. 1981), and has been detected in all of the subsequent observations performed by X-ray satellites with imaging capabilities above 2 keV (Kawai et al. 1988; Sunyaev et al. 1991; Pavlinsky et al. 1994; Lu et al. 1996; Cremonesi et al. 1999; Porquet et al. 2003; Muno et al. 2009; Bird et al. 2010). Its position has been determined with *Chandra* to be $\alpha_{J2000} = 17^{\rm h}\,46^{\rm m}\,21\overset{\rm s}{.}09$, $\delta_{J2000} = -28°43'\,42\overset{''}{.}67$ with a reported $0\overset{''}{.}21$ 1σ accuracy (Evans et al. 2010). Because of its high column absorption ($N_{\rm H} = 1.3 \pm 0.1 \times 10^{23}$ cm^{-2}; see Cremonesi et al. 1999), the source is likely in the Galactic Center ($d = 7.9 \pm 0.3$ kpc; McNamara et al. 2000) or beyond, while the orbital inclination is smaller than 70° (Cowley et al. 1983). The analysis performed by Porquet et al. (2003) detected no pulsations or quasi-periodic oscillations in the 2.4 mHz–2.5 Hz frequency range using EPIC-MOS and the PN fullframe mode (time resolution 2.6 s and 200 ms, respectively). However, since many X-Ray binaries present quasi-periodic variations above 2.5 Hz, the *XMM-Newton* data were not suitable to probe the millisecond pulsations that could indicate a low-mass X-ray binary (LMXB) nature. In their analysis, Porquet tested several single-component spectral models (i.e., absorbed power law, absorbed blackbody, absorbed disk blackbody) but could not distinguish between these models due to the narrow bandpass from 2 to 10 keV. In this regard, *NuSTAR*'s ability to perform high-resolution, broadband spectroscopy allows us to probe more deeply the nature of the high-energy emission from this source.

The presence of an accreting object is required to explain the unabsorbed source luminosity, which is of the order of $L_{2-10\,\rm keV} \sim 10^{36}\, d^2_{10\,\rm kpc}$ erg s^{-1}, where $d_{10\,\rm kpc}$ is the source distance expressed in units of 10 kpc, while the absence of periodic oscillations and eclipses favors a scenario in which a compact object (either a neutron star (NS) or a black hole) accretes matter from a low-mass companion (LMXB systems). LMXBs in this luminosity range which contain an NS are usually characterized by thermonuclear flashes of accreted matter that ignites on the NS surface (Type 1 X-ray bursts), but these bursts have never been observed for 1E1743.1-2843 in 20 years of X-ray observations. So far, this has led to the conclusion that (1) the accretion rate is high enough to allow stable burning of the accreted material, which would imply an $\dot{M}$ value comparable to the Eddington limit (Bildsten 2000), and thus a distance greater than 8 kpc, (2) the bursts are suppressed by the presence of intense magnetic fields (at least

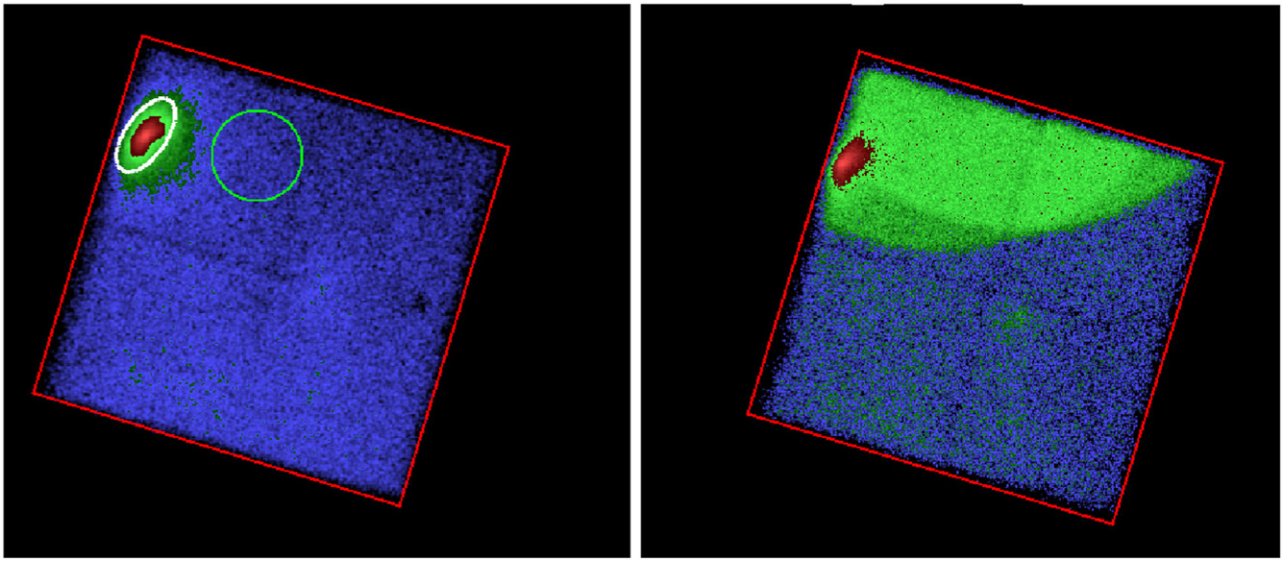

Figure 1. Images from *NuSTAR* focal plane modules in the 3–79 keV energy band, FPMA (left) and FPMB (right); the target source is $\sim 7'$ off-axis during the observation. FPMB is highly contaminated by stray light, and moreover the source is cut in half by two different stray light zones, and therefore only data from FPMA were used in the analysis.

Table 1
NuSTAR and *XMM-Newton* observations of 1E1743.1-2843

Obs.Id	Revolution	Satellite	Start (UTC)	End (UTC)	Exposure Time (s)
40010005001	…	*NuSTAR*	2012 Oct 15 13:31:07	2012 Oct 16 05:41:07	25993
0694640401[a]	2332	*XMM-Newton*	2012 Sep 02 19:33:02	2012 Sep 03 11:20:55	24830
0694640501	2334	*XMM-Newton*	2012 Sep 05 21:16:14	2012 Sep 06 09:46:55	29581
0694641201	2344	*XMM-Newton*	2012 Sep 26 06:17:37	2012 Sep 26 17:24:59	35540

Note. [a] Data from obs. 0694640401 were not used in the analysis.

10^9 G), and (3) the accreting compact object is a black hole (Porquet et al. 2003; Del Santo et al. 2006). The presence of strong magnetic fields ($>10^{12}$ G), however, should be accompanied by cyclotron absorption features and pulsations, neither of which have been observed in 1E1743.1-2843. The source showed marginal variability on month timescales in the 20–40 keV range (Del Santo et al. 2006), some variability on hour timescales (10%–20%) in the 1.3–10 keV energy range (Cremonesi et al. 1999), and less than 18% of variability between 10^{-4} and 2.5 Hz in the 2–10 keV energy range (Porquet et al. 2003).

Here, we present the results of four observations of 1E1743.1-2843 performed with the *NuSTAR* and *XMM-Newton* satellites in 2012 September–October. The two satellites provided almost simultaneous broadband X-ray spectroscopy from 0.1 to 79 keV and, thanks to *NuSTAR*'s timing capabilities, we can also probe pulsations down to 2 millisecond timescales, providing unprecedented opportunities to investigate this source. In Section 2, we describe the observations, and in Section 3 we discuss the timing and spectral analysis. Our results and discussion are presented in Section 4.

2. OBSERVATIONS

All of the observations were performed between 2012 September and October. *NuSTAR* observed 1E1743.1-2843 during the so-called "mini-survey" of the Galactic Center, which took place shortly after the *NuSTAR* in-orbit checkout. The observation was performed on 2012 October 15th, and the total exposure time was 26 ks. The source was $\sim 7'$ off-axis in the *NuSTAR* observation and appears distorted due to the asymmetric point-spread function (PSF) shape at a large off-axis angle (Madsen et al. 2015), as can be seen in Figure 1.

NuSTAR is the first X-ray satellite with multilayer hard X-ray optics and is operational in the energy range 3–79 keV (Harrison et al. 2013). The mission carries two identical telescopes with grazing incidence optics, each one focusing on separate detector modules, Focal Plane Modules A and B (FPMA, FPMB), at a distance of 10 m. These CdZnTe detectors have a total field of view (FOV) of $13' \times 13'$ (Harrison et al. 2013). The telescope PSF has an $18''$ FWHM with extended tails resulting in a half-power-diameter of $58''$ (Harrison et al. 2013).

To improve the low-energy sampling of the source spectrum, we looked for other high-energy observations of 1E1743.1-2843 that were performed during approximately the same period. We adopted three *XMM-Newton* observations performed in imaging mode during 2012 September for a total exposure time of 90 ks. Observation 0694640401, however, is strongly contaminated by solar emission, and we therefore decided to not use it, reducing the useful exposure time to 65 ks. The *XMM-Newton* EPIC-pn camera provides data with nominal accuracy in the 0.3–10 keV energy band (XMM-Newton Science Operations Centre Team 2014), providing a good overlap with the *NuSTAR* data, and thereby minimizing possible bias in the spectral modeling.

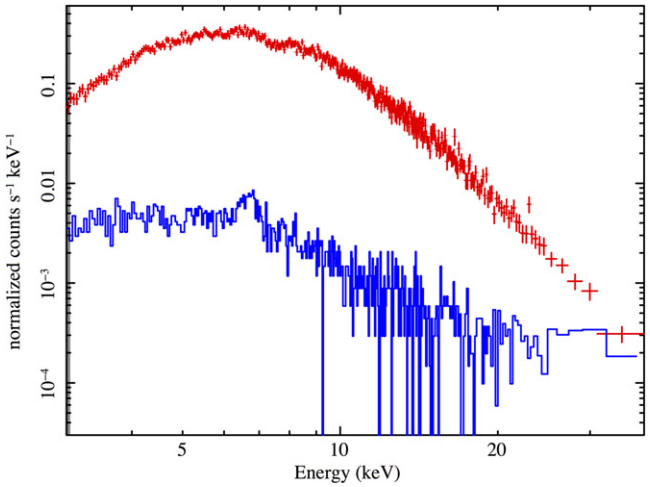

Figure 2. Spectrum acquired from the *NuSTAR* FPMA extraction region. The red crosses indicate the source spectrum rebinned to have at least 5σ significance and 30 counts for each bin. The blue line is the background spectrum.

The *NuSTAR* observations are not simultaneous with *XMM-Newton*. However, due to the small difference in time (a few weeks, see Table 1), and since 1E1743.1-2843 does not usually exhibit substantial spectral variability (Cremonesi et al. 1999), we jointly fit the two data sets with a cross-normalization factor to account for any flux variation. During the observations, the difference in source flux measured by the two instruments in the overlapping energy band (3–10 keV) was below 1.3%, indicating a good compatibility of the data sets.

3. DATA ANALYSIS

3.1. NuSTAR

We analyzed the *NuSTAR* data set (obsID 40010005001) using the *NuSTAR* Data Analysis Software (NuSTARDAS) version 1.3.1 (2013 December 9), HEASOFT 6.15.1, and the most up-to-date calibration files and responses. The software applies offset correction factors to the energy response to account for the movement of the mast which causes a varying position of the focal spots on the detector planes. For the data from each of the two modules, the pipeline produces an image, spectrum, and deadtime-corrected light curve. For each *NuSTAR* observation, the source and background subtraction regions must be carefully evaluated due to the possible presence of contaminating sources outside the FOV that induce stray light patterns on the detectors. Unfortunately the *NuSTAR* detectors are not entirely shielded from unfocused X-rays, and this stray light can be significant if there are bright X-ray sources within ~2°–3° of the pointing direction (Krivonos et al. 2014; Wik et al. 2014; Mori et al. 2015). In this observation, FPMB is highly contaminated by two different stray light patterns, as can be seen in Figure 1, and furthermore the source focal spot straddles the two different patterns. Due to the complexity of separating the source emission from the stray light, we decided to discard all of the data from FPMB.

The source spectra are shown in Figure 2 and were obtained by extracting photons in an elliptical region of 95″ × 46″ semi axis, rotated by 35° clockwise relative to north and centered on the source centroid, and by subtracting the count rate measured in a nearby circular background region of radius 114″ (see Figure 1). The different area normalizations were taken into account in the background subtraction. The dead layer thickness of the two modules varies depending on the location on the detector and, since the pipeline could fail to correct the response matrix for this effect to a suitable accuracy for high off-axis angles, we decided to ignore the data below 5 keV. Also, due to imperfect background subtraction, the data above 40 keV were ignored. All of the data bins were grouped to reach at least 30 counts. The total source count rate in this energy range is 2.10 ± 0.01 cts s^{-1}.

3.2. XMM-Newton

We extracted the spectra of the EPIC-pn camera in the 0.3–10 keV energy range following the standard procedure described in the *XMM-Newton* software analysis guide[13] for observations 0694640401, 0694640501, and 0694641201, using the SAS software release xmmsas_20131209_1901-13.5.0. The light curves and spectra of 1E1743.1-2843 were extracted from annular extraction regions excluding those zones where the number of counts exceeded 800 to avoid pileup if present (see Figure 3). The light curves are shown in Figure 4.

EPIC-pn data below 0.3 keV are mostly related to artifacts and noise and were excluded (XMM-Newton Science Operations Centre Team 2016), and all the bins were grouped to reach at least 30 counts. The mean count rate for the two observations is 2.62 ± 0.01 cts s^{-1}.

3.3. Timing Analysis

A light curve of the *NuSTAR* observation with 10 ms time bin resolution was extracted for FPMA in the energy[14] range 3–60 keV using *nuproducts*. Timing data were corrected for deadtime and for arrival times at the Solar System barycenter using the JPL 2000 ephemeris (Standish 1982; for this purpose, we used the barycorr tool in the HEASOFT 6.16 distribution). We then calculated the power spectra on different contiguous time intervals and averaged them into a total spectrum. Each single spectrum was built using intervals of 32,768 bins, and the total spectrum was built averaging 87 intervals in a single frame. This was finally rebinned in frequency channels for more statistics. An offset constant term was subtracted from the total spectrum to remove the Poisson noise level and compensate for residual effects of the deadtime correction (this term was evaluated as the average power in the frequency interval 10–49 Hz). The resulting power spectrum is shown in Figure 5. The statistics is too poor to model the power spectrum with a multi-parameter function (such as a Lorentzian). Signal is detected only up to frequencies of ~0.1 Hz, with some hint of complex structure, like the presence of a possible break at frequencies >0.02 Hz.

We also performed a Lomb–Scargle periodogram of the same frequency interval as the power spectrum and found no significant signal. The power spectrum and Lomb period analysis were also performed for the two *XMM-Newton* observations, also yielding no positive detection of periodicities.

[13] ftp://legacy.gsfc.nasa.gov/xmm/doc/xmm_abc_guide.pdf The *XMM-Newton* ABC Guide: An Introduction to *XMM-Newton* Data Analysis.

[14] The low-energy range is different from that used in the spectral analysis section, in the attempt to maximize the S/N.

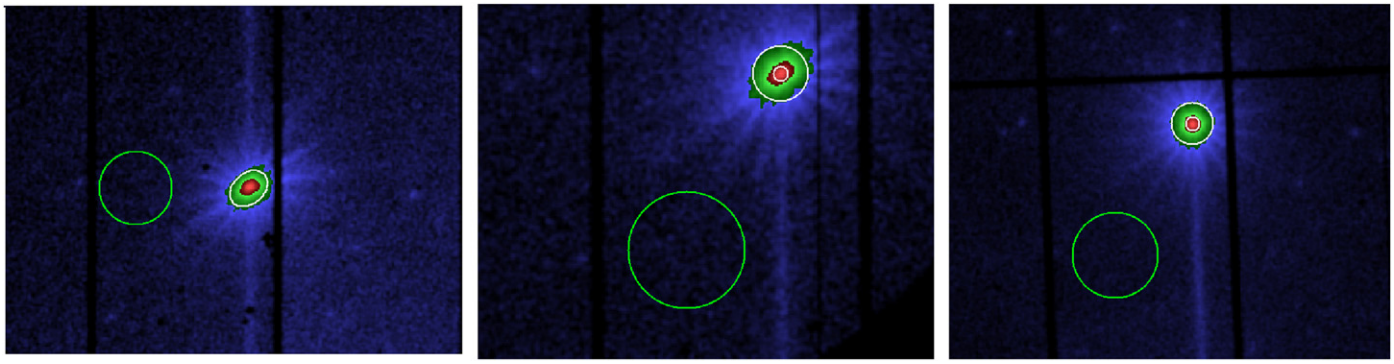

Figure 3. Images of 1E1743.1-2843 from the *XMM-Newton* EPIC-pn camera. White ellipses show the annular extraction region and green circles show the background regions. The bright central zone of the source was excluded due to pileup in the central and rightmost panels, while the pileup threshold was not exceeded in the leftmost one (thus no inner ellipse was plotted on the image).

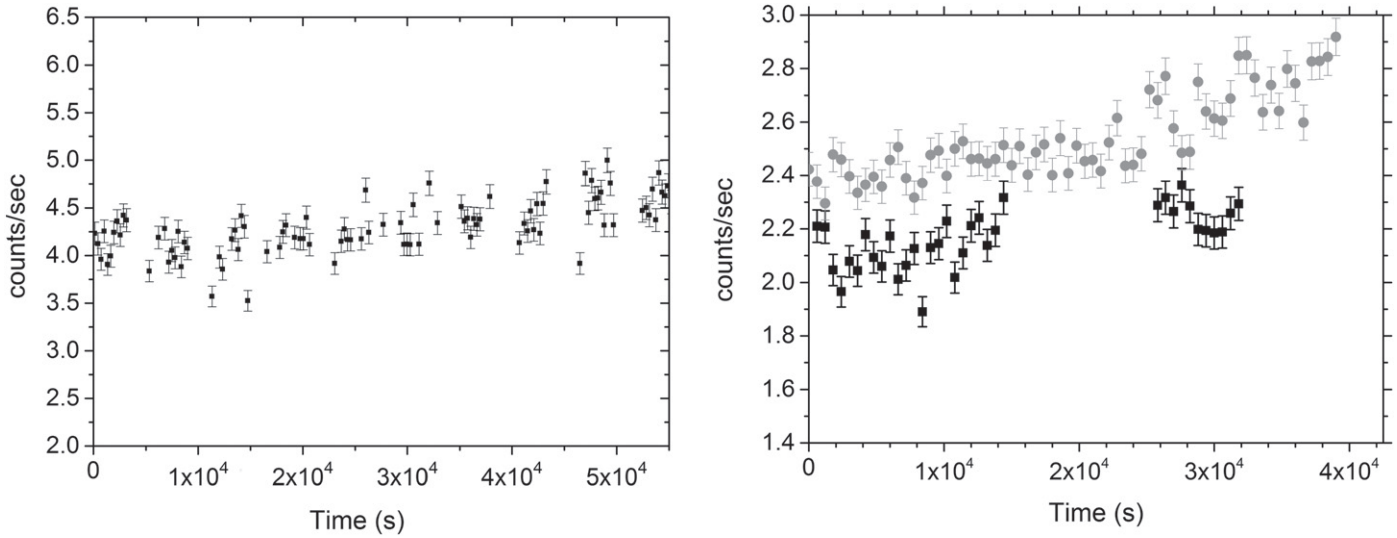

Figure 4. Light curves of 1E1743.1-2843 acquired from the *NuSTAR* FPMA in the 3–80 keV energy range (left, 300 s bins), and from the two *XMM-Newton* analyzed observations in the 0.3–10 keV energy range (right, 600 s bins, observation 0694640501 and 0694641201 in black and gray, respectively).

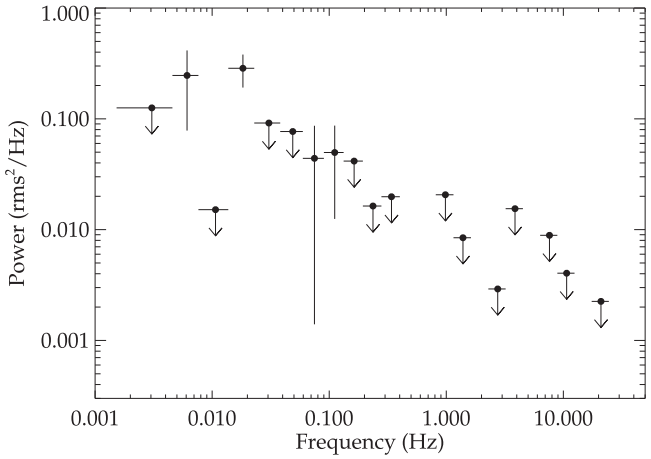

Figure 5. Power spectrum of the *NuSTAR* observation of 1E1743.1-2843, with indication of a low frequency break at frequencies >0.02 Hz. Upper limits are 1σ.

3.4. Spectral Analysis

We analyzed the *NuSTAR* and *XMM-Newton* data sets using XSPEC (Arnaud 1996) version 12.8.0, using the `TBabs` with abundances set as in Wilms et al. (2000), and cross-sections set as in Verner et al. (1996) to model the effect of X-ray absorption. We performed the fit allowing for the normalizations among the three different observations to vary. These normalizations relative to the different *XMM-Newton* data sets remained constant for every model and were found to be $C_1 = 0.99 \pm 0.01$, $C_2 = 1.00 \pm 0.01$ for observations 0694641201 and 0694640501, respectively.

We used the following four models to determine the nature of the source, the first three of which were used to test the origin of the low-energy emission.

1. Model 1: a blackbody (`bbodyrad`) and a power law with a high-energy cutoff (`power law × highEcut`). This is a typical single-component spectral model and assumes that the source is an NS binary.
2. Model 2: a disk blackbody (`diskbb`) plus a `power law × highEcut`. This is also a typical single-component spectral model but assumes that the compact source is a black hole binary.
3. Model 3: a disk blackbody (`diskbb`), a blackbody (`bbodyrad`), and the `power law × highEcut`. This model probes deeper into the NS hypothesis, adding an accretion disk component to model 1.

Table 2
Fit Results of the *NuSTAR* and *XMM-Newton* Observations

XSPEC Model	Parameter	Units	Model 1	Model 2	Model 3	Model 4
TBabs	$N_{\rm H}$	10^{22} cm^{-2}	$14.8^{+0.9}_{-0.8}$	16.6 ± 0.5	$16.5^{+1.0}_{-1.3}$	$15.3^{+0.8}_{-1.1}$
bbodyrad	kT	keV	1.8 ± 0.1	…	$1.8^{+0.1}_{-0.2}$	1.83 ± 0.05
bbodyrad	norm[a]	…	$1.3^{+0.5}_{-0.3}$	…	1.0 ± 0.3	$1.7^{+0.4}_{-0.2}$
diskbb	$kT_{\rm in}$	keV	…	$2.4^{+0.2}_{-0.3}$	$0.12^{+0.04}_{-0.02}$	$0.12^{+0.04}_{-0.03}$
diskbb	norm[b]	…	…	$0.19^{+0.1}_{-0.08}$	…	…
power law	Γ	…	$1.0^{+0.3}_{-0.5}$	$0.9^{+0.3}_{-0.4}$	$1.3^{+0.2}_{-0.3}$	…
power law	norm[c]	…	$0.009^{+0.007}_{-0.006}$	$0.01^{+0.01}_{-0.005}$	0.02 ± 0.01	…
highecut	cutoffE	keV	6.6 ± 0.4	6.9 ± 0.30	$7.2^{+0.4}_{-0.7}$	…
highecut	foldE	keV	$8.1^{+1.7}_{-1.5}$	$6.3^{+0.5}_{-1.3}$	$9.0^{+1.8}_{-1.3}$	…
compTT	T_0	keV	…	…	…	$0.014^{+8.4}_{-2.9}$
compTT	kT	keV	…	…	…	$4.6^{+0.6}_{-0.4}$
compTT	τ_p	…	…	…	…	$6.2^{+6.5}_{-1.4}$
compTT	norm[d]	…	…	…	…	$0.031^{+93}_{-0.013}$
$\frac{\chi^2}{dof}$	…	…	$\frac{2798.3}{2637}$	$\frac{2835.4}{2637}$	$\frac{2766.4}{2635}$	$\frac{2785.0}{2635}$
reduced χ^2	…	…	1.061	1.075	1.050	1.057

Notes. The errors are expressed with 90% confidence. Parameters not reported were not constrained by the fit.
[a] $R^2_{\rm km}/D^2_{10}$, where $R_{\rm km}$ is the source radius in km and D_{10} is the distance to the source in units of 10 kpc.
[b] $(R_{\rm in[km]}/D_{10})^2 \cos\theta$, where $R_{\rm in[km]}$ is the apparent disk radius and θ is the angle of the disk ($\theta = 0$ is face-on).
[c] The power-law component normalization in units of photons keV^{-1} cm^{-2} s^{-1}.
[d] The thermal Comptonization component normalization in units of photons keV^{-1} cm^{-2} s^{-1}.

4. Model 4: a disk blackbody (`diskbb`), a blackbody (`bbodyrad`), and the `compTT` Comptonization model. In this model, the power law in model 3 is replaced by a more physical model.

To model the emission from the accretion disk, we used the multi-color `diskbb` model mentioned before (Mitsuda et al. 1984; Makishima et al. 1986).

The fit results shown in Table 2 indicate that the source emission is mainly contributed by a prominent blackbody component at ∼2 keV plus a high-energy continuum which can be described equally well by an empirical law (`power law × highEcut`) or by a thermal Comptonization (`compTT`) component. As can be seen from Table 2, all of the models provide a good fit for the data. In the following, we will assume model 3 as our baseline, since it provides the lowest χ^2 value, and a reasonable physical interpretation of the data, as discussed in Section 4.

Adding another absorption component with partial covering (`pcfabs`) to model 1 did not improve the fit results, and therefore we conclude that the source is not partially obscured. Also, the spectroscopic data do not require the addition of further high-energy components such as, for instance, reflection, as we verified by adding the `coplrefl` (Ballantyne et al. 2012) reflection component to model 3.

We then addressed the high-energy component taking as a baseline model 3 and replacing the power-law plus cutoff component with a more physical model, specifically, `compTT` (Titarchuk 1994), which describes the Comptonization of soft photons in a thermal plasma of high-energy electrons above the accreting source. In the resulting model 4, the `compTT` component gives a worse fit than the power law with an exponential cutoff (model 3). However, model 4 still yields a better fit than models 1 and 2, and has the advantage of allowing a more physical interpretation of the source spectrum than the empirical model 3. Furthermore, we tested if a single thermal component and a Comptonized component could fit the data, and replaced the power law in model 1 with the `compTT` model. However, this resulted in a worse fit ($\chi^2_{\rm red} \sim 1.07$). Finally, if we test model 4 for the presence of the fluorescence line of neutral iron, $\chi^2_{\rm red}$ rises to 1.2. Therefore, the presence of the iron K_α line is also not required. From model 4, we derive an upper limit on the iron K_α equivalent width (EW) of 4.9 eV.

Summarizing, model 3 and model 4 give the best results. Model 3 has the lower reduced χ^2 value between the two, although the `compTT` model allows the determination of the physical parameters of the source. The resulting spectra for model 4 are shown in Figure 6, and the results of the overall fits are reported in Table 2.

4. DISCUSSION

In this work, we have reported on a broadband (0.3–40 keV) spectral analysis of 1E1743.1-2843, which was observed with *NuSTAR* and *XMM-Newton*. A similar analysis was previously performed using *INTEGRAL* data (Del Santo et al. 2006), but the improved energy resolution and sensitivity of *NuSTAR* allow us to better constrain the hard X-ray continuum, identifying the presence of Comptonization and of a cutoff in the high-energy emission for the first time. This allowed us to use more sophisticated models compared to previous works (Cremonesi et al. 1999; Porquet et al. 2003; Del Santo et al. 2006). Below, we summarize the results obtained and discuss those which support either the LMXB or high-mass X-ray binary (HMXB) nature of the system.

Regarding the low-energy emission of the source, the presence of the $kT = 1.8$ keV blackbody is a strong indication of an NS nature of the compact object. The blackbody radius is ∼1 km if we assume the source to be located in the Galactic Center, at $d \sim 8.8$ kpc. This is not compatible with emission from a boundary layer near the NS surface ($R_{\rm BL} - R_{\rm NS} \sim 2$ km for low $\dot{M}$, Popham & Sunyaev 2001), but is consistent with emission from a restricted region of the NS surface (i.e., from an equatorial belt in the orbital plane, or with magnetically

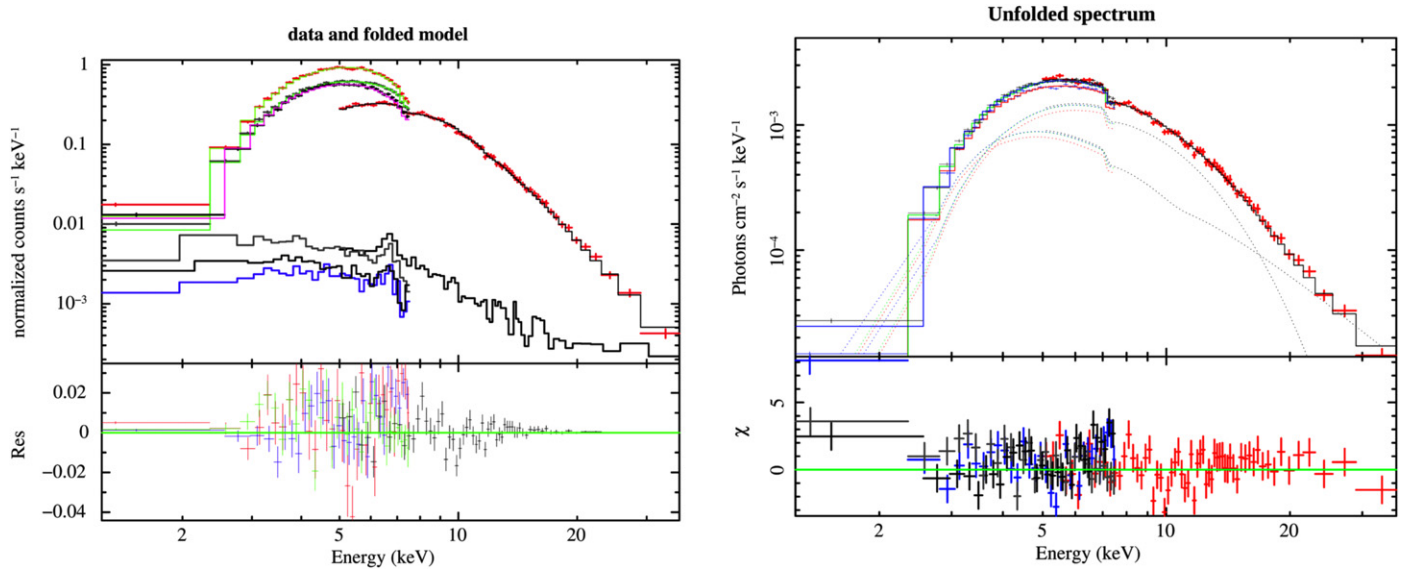

Figure 6. Left—folded spectra, backgrounds, and residuals with respect to model 4 for all of the spectra analyzed. Right—the analyzed spectra, unfolded through model 4. The plots are rebinned in groups of 30 channels for display purposes.

driven accretion onto polar caps). In the latter case, the magnetic field strength of the compact source should be $>10^9$ G. There may be soft excess which could be interpreted as weak emission from an accretion disk ($kT \sim 0.1$ keV). However, the *XMM-Newton* data were unable to constrain the blackbody normalization due to the high hydrogen column absorption ($N_{\rm H} \sim 1.6 \times 10^{23}$ cm^{-2}). In the HMXB scenario, this soft excess could also be interpreted as a blend of emission lines, as thermal emission from the NS surface, or Thomson scattering of the hot spot emission by the accreting material (van der Meer et al. 2004). The reliability of the soft excess detection is worth discussing because the χ^2 improvement it provides is moderate. The use of the F-test could result in unreliable results (Protassov & van Dyk 2002), and so we performed a series of Monte Carlo simulations with the *simftest* routine to confirm the presence of such a component, following the approach described by Bhalerao et al. (2015). The highest $\Delta\chi^2$ obtained in 10,000 simulations is 18.7, which is significantly lower than the $\Delta\chi^2 = 43.2$ obtained by the real data (see Figure 7). We estimate that $>10^9$ simulations would be required to get $\Delta\chi^2 > 40$, corresponding to a significance higher than 6σ. Nevertheless, even if the presence of the soft excess is statistically preferred, then we cannot exclude that the low-energy spectrum is affected by systematics, which could arise, e.g., in adding two exposures taken at different epochs. We regard this as a result that needs to be confirmed by better-quality, low-energy data from future observations of this source.

The presence of a neutral iron K_α line at 6.4 keV is not statistically required, with an upper limit on the EW of 4.9 eV from model 4 (6.7 eV from model 3). This value is compatible with the expected properties of LMXBs (Asai et al. 2000) and radio-quiet quasars (George et al. 2000), as already pointed out by Porquet et al. (2003). This weakens the HMXB hypothesis for this source, since the iron line is usually detected in such systems. On the other hand, the lack of the Fe K_α line in LMXBs is very common, and is usually associated with the Baldwin effect: the high luminosity of the X-ray source increases the degree of iron ionization (Torrejón et al. 2010).

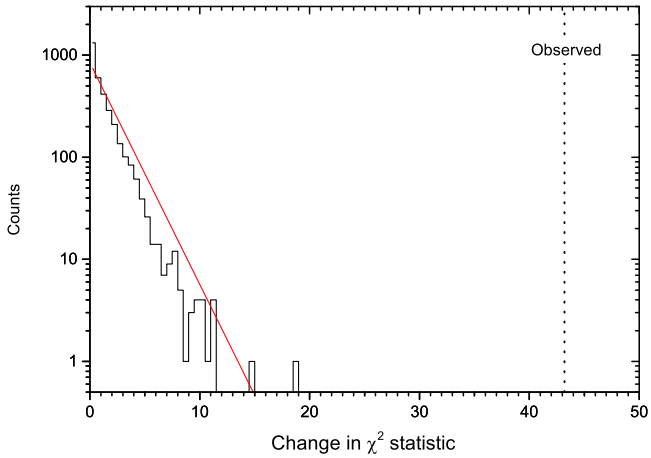

Figure 7. Results of Monte Carlo simulations for testing the presence of the disk component. We simulated the spectra from model 3 without (our null-hypothesis) and with the disk component. The histogram shows the $\Delta\chi^2$ obtained in 10,000 simulations (in black), together with the $\Delta\chi^2$ distribution expected from the addition of 2 free parameters (red line). The vertical dashed line is the $\Delta\chi^2$ value obtained from the actual data (43.19).

The high-energy emission is characterized by a power law ($\Gamma \sim 1.3$) with a high-energy cutoff ($E_{\rm cut} \sim 7.2$ keV), identified for the first time thanks to the *NuSTAR* hard X-ray sensitivity. The *NuSTAR* data also unambiguously identified the presence of a Comptonization component induced by an electron population with a temperature of a few keV ($kT_0 \sim 4.6$ keV, in accordance with the exponential cutoff value found), indicating a large viewing angle (see Matsuoka & Asai 2013). Even if X-rays are produced near the NS at energies of several tens of keV, the observed X-rays will be shifted to lower energy due to Comptonization by the more distant low-energy plasma with a temperature of several keV. This Comptonization component has a strong interplay with the 1.8 keV blackbody up to ~20 keV, since the total hard X-ray spectrum cannot be described as a single power law. We tested for the presence of a reflection component, and found that it is not required to explain the data. A fit with a power-law model

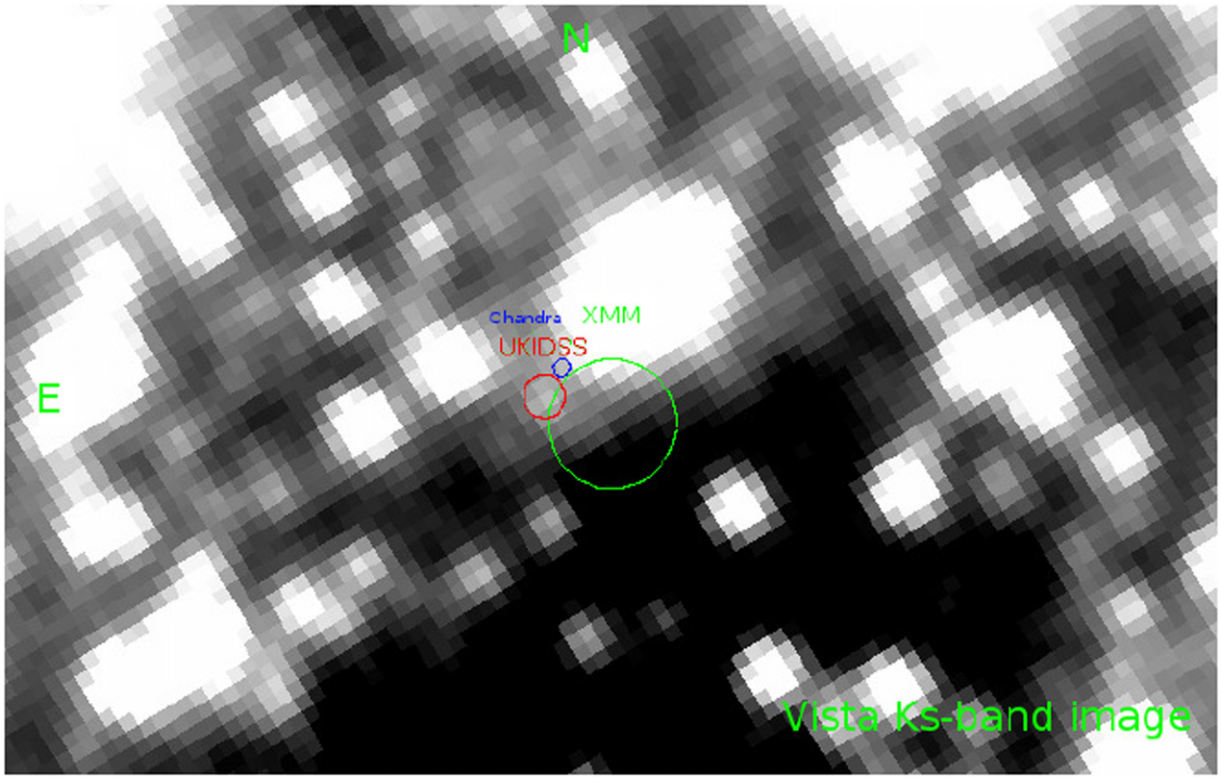

Figure 8. *Ks*-band image of 1E1743.1-2843 obtained with Vista. The *Chandra* and *XMM-Newton* positions of 1E1743.1-2843 are shown, together with the position of UGPS J174621.12284343.3 as reported in the UKIDSS catalog (coordinates: R.A. = 17:46:21.13, $\delta = -28$:43:43.17 J2000). The *Chandra* error circle excludes the possibility of this source being the counterpart.

without breaks brought higher values of the photon index ($\Gamma = 2.3^{+0.08}_{-0.09}$), which are compatible with previous results (Cremonesi et al. 1999; Porquet et al. 2003; Del Santo et al. 2006), but also produced a higher value of the $\chi^2/\mathrm{dof} = 2880.79/2639 = 1.09$ compared to that obtained with the high-energy cutoff ($\chi^2_{\mathrm{red}} = 1.05$; see Table 2), indicating that using the former description for the higher-energy data is marginally justified at best.

The source luminosity is $L_{2-10\,\mathrm{keV}} \sim 1.5 \times 10^{36}\, d^2_{10\,\mathrm{kpc}}$ erg s^{-1}, so that if we assume that the source is located in the Galactic Center, then we obtain $L_{2-10\,\mathrm{keV}} \sim 10^{36}$ erg s^{-1}, which is within the typical range of luminosity for X-ray bursters (Cremonesi et al. 1999; Bildsten 2000). To investigate further, we have extracted the *Ks*-band image of the Vista survey "VISTA Variables in the Via Lactea (VVV)" (Minniti et al. 2010; see Figure 8). Both the *XMM-Newton* and *Chandra* positions of 1E1743.1-2843 are visible in the image, as is the position of the source UGPS J174621.12284343.3 as reported in the UKIDSS catalog (Lawrence et al. 2008). The nominal accuracy of UKIDSS is ∼0.1 arcsec, but to account for source confusion in this crowded region we used a larger 0.3 arcsec positional error, as suggested by Lucas et al. (2008). We should consider whether this source might be the counterpart. In the UKIDSS catalog, this source does not have a *K*-band magnitude listed, but it has $H = 16.82 \pm 0.09$ and $J = 18.39 \pm 0.08$. Assuming a $0\farcs21$ uncertainty on the *Chandra* position (Evans et al. 2010), then this source is excluded, as can be seen in the figure. Also, given the extreme IR source crowding in the GC, the fraction of true-to-candidate counterparts for hard *Chandra* sources is very low (see, for instance De Witt et al. 2010). Furthermore, since the *NuSTAR*/*XMM-Newton* column densities are consistent with the overall Galactic Center value, it is not likely that the companion star is hidden by a cloud either. However, we cannot exclude a high-mass companion solely on the basis of the absence of a bright IR source. In fact, a B-type star placed at the distance of 8.5 kpc could have IR magnitudes fainter than the limiting H-band magnitude of the vista surveys of the Galactic Center (McMahon et al. 2013), assuming an IR absorption corresponding to the hydrogen column density we measured for 1E1743.1-2843 (see Table 2).

In the LMXB hypothesis, the fact that not a single burst has been observed in over 20 years suggests that the source is a rare burster (in't Zand et al. 2004). In principle, the lack of bursts could be explained if the source is located outside the Galaxy. Specifically, to reach $L = 2.9 \times 10^{37}$ erg s^{-1}, corresponding to the stable burning of accreted material, 1E1743.1-2843 would need to be placed at $d \sim 40$ kpc. However, a study of the stability conditions for accreting objects (Narayan & Heyl 2002) indicates that, for an NS with a surface temperature of ∼2 keV, there is a luminosity range where stable accretion is possible between the instability regions where He and H bursts are triggered. This "stability strip" corresponds roughly[15] to luminosities $1.3 \times 10^{36} < L < 6.5 \times 10^{36}$ erg s^{-1}. This implies that if the source is located between the Galactic Center and ∼16 kpc, the lack of bursts is to be expected, as is the lack of the detection of an IR companion.

Church et al. (2014) recently proposed a unified model for the LMXB sources. The model assumes the presence of an extended accretion disk corona (ADC). For

[15] Exact boundaries depend weakly on the NS radius.

$L > 1$–2×10^{37} erg s^{-1}, the ADC is in thermal equilibrium with the NS surface, giving rise to a Comptonized spectrum with $E_{\rm cut} \sim 6$ keV, which corresponds roughly to three times the actual temperature of the electrons (in the assumption of high optical depth). For lower luminosities, Comptonization becomes inefficient in cooling the corona, the thermal equilibrium assumption breaks down, and, as a consequence, the extended ADC heats up to several tens of keV. In this scenario, the ∼1 km blackbody radii in LMXBs are explained by an emitting region in the shape of an equatorial strip in the orbital plane with a half height of $h \sim 100$ m. This scenario is described by a blackbody plus a cutoff power law (our model 1). The authors also note that compTT is not consistent with the evidence for an extended corona. The outer regions of the accretion disk ($kT \sim 0.1$ keV), which provide the seed photons for Compton scattering, are not expected to be detected. Our results for the blackbody temperature ($kT \sim 1.8$ keV) and radius ($r \sim 1$ km), for the $E_{\rm cut} \sim 3kT_{e^-} \sim 6.6$ keV of the Comptonized component, and for the ratio of total to blackbody luminosity for 1E1743.1-2843 fit within the expected ranges for the scenario they depict as the Banana state of the Atoll sources. This interpretation, however, implies $L > 2 \times 10^{37}$ erg s^{-1} to explain the spectral cutoff value and the lack of bursting activity. This would require a distance of a few tens of kiloparsecs to account for the observed flux, which could be explained if 1E1743.1-2843 were in the Sagittarius dwarf elliptical galaxy (SAGDEG), one of the small dwarf spheroidal galaxies that orbit the Milky Way. SAGDEG is currently behind the GC at a distance of $d \sim 26$ kpc (Cole et al. 2009), and is in an advanced state of destruction due to tidal interactions with the Galaxy. Therefore, a fraction of the stars that composed this dwarf galaxy have likely scattered to even greater distances.

In the HMXB scenario, the presence of a strong magnetic field ($B \sim 10^{12-13}$ G) suppresses the propagation of the bursts across the NS surface (Gilfanov & Sunyaev 2014). However, the lack of eclipses, an Fe K_α line, and pulsations in the light curve, as well as the missing detection of a companion star, make the HMXB hypothesis less favored, even though the value of the spectral cutoff (9 ± 1.8 keV) is compatible with that expected from HMXBs (10–20 keV).

We conclude that while an HMXB framework leaves several unexplained features, interpreting 1E1743.1-2843 as an NS-LMXB scenario is more consistent, implying a peculiar but not unique object. In this case, the source could be located at a distance of $9 < d < 16$ kpc, between the two instability luminosity intervals where He and H bursts are triggered, or, if we rely on the unified model proposed by Church et al. (2014), at a distance of $d > 36$ kpc, corresponding to the stable burning of accreted material.

This work was supported under NASA Contract No. NNG08FD60C and made use of data from the *NuSTAR* mission, a project led by the California Institute of Technology, managed by the Jet Propulsion Laboratory, and funded by the National Aeronautics and Space Administration. We thank the *NuSTAR* Operations, Software, and Calibration teams for support with the execution and analysis of these observations. This research has made use of the *NuSTAR* Data Analysis Software (NuSTARDAS) jointly developed by the ASI Science Data Center (ASDC, Italy) and the California Institute of Technology (USA). The Italian authors acknowledge the Italian Space Agency (ASI) for financial support by ASI/INAF grant I/037/12/0. R.K. acknowledges support from Russian Science Foundation (grant 14-22-00271).

REFERENCES

Arnaud, K. A. 1996, in ASP Conf. Ser. 101, Astronomical Data Analysis Software and Systems V, ed. G. H. Jacoby, & J. Barnes (San Francisco, CA: ASP), 17
Asai, K., Dotani, T., Nagase, et al. 2000, ApJS, 131, 571
Ballantyne, D. R., Purvis, J. D., Strausbaugh, R. G., et al. 2012, ApJL, 747, L35
Bhalerao, V., Romano, P., & Tomsick, J. 2015, MNRAS, 447, 3
Bildsten, L. 2000, in AIP Conf. Proc. 522, Cosmic Explosions: Tenth Astrophys. Conf, ed. S. S. Holt, & W. W. Zhang (Melville, NY: AIP), 359
Bird, A. J., Bazzano, A., & Bassani, L. 2010, ApJS, 186, 1
Church, M. J., Gibiec, A., & Bałucińska-Church, M. 2014, MNRAS, 438, 4
Cole, N., Newberg, H. J., Magdon-Ismail, M., et al. 2009, in ASP Conf. Ser. 411, Astronomical Data Analysis Software and Systems XVIII, ed. D. A. Bohlender, D. Durand, & P. Dowler (San Francisco, CA: ASP), 221
Cowley, A. P., Crampton, D., Hutchings, J. B., et al. 1983, ApJ, 272, 118
Cremonesi, D., Mereghetti, S., Sidoli, L., & Israel, G. L. 1999, A&A, 345, 826
Del Santo, M., Sidoli, L., Bazzano, A., et al. 2006, A&A, 456, 1105
De Witt, C., Bandyopadhyay, R. M., Eikenberry, S. S., et al. 2010, ApJ, 721, 2
Evans, I. N., Primini, F. A., Glotfelty, K. J., et al. 2010, ApJS, 189, 37
George, I. M., Turner, T. J., Yaqoob, T., et al. 2000, ApJ, 531, 52
Gilfanov, M. R., & Sunyaev, R. A. 2014, Physics-Uspekhi, 57, 4
Harrison, F. A., Craig, W. W., Christensen, F. E., et al. 2013, ApJ, 770, 103
in't Zand, J. J. M., Verbunt, F., Heise, J., et al. 2004, NuPhS, 132, 486
Kawai, N., Fenimore, E. E., Middleditch, J., et al. 1988, ApJ, 330, 130
Krivonos, R. A., Tomsick, J. A., Bauer, F. E., et al. 2014, ApJ, 781, 107
Lawrence, A., Warren, S. J., Almaini, O., et al. 2008, MNRAS, 379, 1599
Lu, F. J., Li, T. P., Sun, X. J., et al. 1996, A&A, 115, 395
Lucas, P. W., Hoare, M. G., Longmore, A., et al. 2008, MNRAS, 391, 136
Madsen, K., Harrison, F. A., & Markwardt, C. 2015, ApJS, 220, 1
Makishima, K., Maejima, Y., Mitsuda, K., et al. 1986, ApJ, 308, 635
Matsuoka, M., & Asai, K. 2013, PASJ, 65, 26
Muno, M. P., Bauer, F. E., Baganoff, F. K., et al. 2009, ApJS, 181, 1
McMahon, R. G., Banerji, M., Gonzalez, E., et al. 2013, Msngr, 154, 35
McNamara, D. H., Madsen, J. B., Barnes, J., et al. 2000, PASP, 112, 202
Minniti, D., Lucas, P. W., Emerson, J. P., et al. 2010, NewA, 15, 433
Mitsuda, K., Inoue, H., Koyama, K., et al. 1984, PASJ, 36, 74
Mori, K., Hailey, C. J., Krivonos, R., et al. 2015, ApJ, 814, 2
Narayan, R., & Heyl, J. S. 2002, ApJL, 574, L139
Pavlinsky, M. N., Grebenev, S. A., & Sunyaev, R. A. 1994, ApJ, 425, 110
Popham, R., & Sunyaev, R. 2001, ApJ, 547, 355
Porquet, D., Rodriguez, J., Corbel, S., et al. 2003, A&A, 406, 299
Protassov, R., & van Dyk, D. A. 2002, ApJ, 571, 545–59
Standish, M. 1982, A&A, 114, 297
Sunyaev, R., Churazov, E. M., Gil'Fanov, M. R., et al. 1991, AdSpR, 11, 177
Titarchuk, L. G. 1994, ApJ, 434, 570
Torrejón, J. M., Schulz, N. S., Nowak, M. A., & Kallman, T. R. 2010, ApJ, 715, 947
van der Meer, A., di Salvo, T., Kaper, L., et al. 2004, NuPhS, 132, 624
Verner, D. A., Ferland, G. J., Korista, K. T., & Yakovlev, D. G. 1996, ApJ, 465, 487
Watson, M. G., Willingale, R., Hertz, P., & Grindlay, J. E. 1981, ApJ, 250, 142
Wik, D. R., Hornstrup, A., Molendi, S., et al. 2014, ApJ, 792, 48
Wilms, Allen, & McCray 2000, ApJ, 542, 914
XMM-Newton Science Operations Centre Team 2016, Issue 12.0, Users Guide to the XMM-Newton Science Analysis System, http://xmm.esac.esa.int/external/xmm_user_support/documentation/sas_usg/USG.pdf